Complete Wetting of Nanosculptured Substrates

M. Tasinkevych[1,2] and S. Dietrich[1,2]

[1]*Max-Planck-Institut für Metallforschung, Heisenbergstrasse 3, D-70569 Stuttgart, Germany*

[2]*Institut für Theoretische und Angewandte Physik, Universität Stuttgart, Pfaffenwaldring 57, D-70569 Stuttgart, Germany*

(Received 11 May 2006; published 7 September 2006)

Complete wetting of geometrically structured substrates by one-component fluids with long-ranged interactions is studied theoretically. We consider periodic arrays of rectangular or parabolic grooves and lattices of cylindrical or parabolic pits. We show that the midpoint interfacial heights within grooves and pits are related in the same way as for complete wedge and cone filling. For sufficiently deep cavities with vertical walls and small undersaturation, an effective planar scaling regime emerges. The scaling exponent is $-1/3$ in all cases studied, and only the amplitudes depend on the geometrical features. We find quantitative agreement with recent experimental data for such systems.

DOI: 10.1103/PhysRevLett.97.106102 PACS numbers: 68.08.Bc, 05.70.Np

The growing interest in device miniaturization has led to the emergence of various experimental techniques of tailoring the geometrical and chemical topography of solid surfaces at mesoscopic scales [1,2]. Such nanopatterning of the surfaces may result in drastic changes of their wetting characteristics, which is important for technologies such as microfluidics [3] or the fabrication of superhydrophobic or superhydrophilic surfaces [2]. Experimental studies of complete wetting on sculptured surfaces [4,5] demonstrate the strong influence of nanocavities on the adsorption behavior relative to that of flat substrates. Theoretical studies of adsorption in infinitely deep generalized wedges [6] predict geometry-dependent wetting exponents.

Although it is known that a nonplanar topography of a substrate modifies its wetting by a fluid, recent studies have revealed surprising hidden symmetries, or so-called covariances, which relate various local adsorption properties for different substrate geometries. These covariances imply that different confining potentials can lead to identical local interfacial properties once external fields are suitably rescaled.

For instance, for both long- and short-ranged forces, complete wetting at the apex of a wedge can be mapped onto critical wetting of a planar substrate with the apex angle playing the role of the contact angle [7], which maps one-to-one to temperature. In two-dimensional systems, critical wedge filling can be related to the strong-fluctuation regime of critical planar wetting [8]. Recently, a new example of geometrical covariance relating wedge and cone complete filling has been reported [9] showing that the equilibrium midpoint interfacial heights $l^{(0)}$ in a cone and a wedge obey the relation $l_c^{(0)}(\Delta\mu, \alpha) = l_w^{(0)}(\Delta\mu/2, \alpha)$ with α being the substrate tilt angle and $\Delta\mu \geq 0$ the chemical potential deviation from liquid-vapor coexistence. This relation is valid for the leading behaviors of l in the limit $\Delta\mu \to 0^+$.

In the following we demonstrate that complete wetting of substrates patterned by periodic arrays of grooves or quadratic lattices of pits (see Fig. 1), both of depths D, exhibits a geometrical covariance similar to the one described in Ref. [9]. We consider rectangular or parabolic grooves and cylindrical or parabolic pits, taking into account the long range of the intermolecular potentials. We observe four different scaling regimes: filling, postfilling, effective planar, and planar, with the neighboring regimes being separated by, as we call, $\Delta\mu_{\rm fil}^{p,g} > \Delta\mu_\pi^e > \Delta\mu_\pi$. The aforementioned covariance relates the behavior of the midpoint wetting film thicknesses for all geometries and holds within an undersaturation range $\Delta\mu_\pi^e \lesssim \Delta\mu \lesssim \Delta\mu_{\rm fil}^{p,g}$ (for $\Delta\mu_\pi^e$ see below; the superscripts p, g refer to pits and grooves, respectively) which we call the *postfilling scaling regime*. In the case of cylindrical pits or rectangular grooves, for $\Delta\mu \searrow \Delta\mu_{\rm fil}^{p,g}(R)$ and for sufficiently large D/R, the analogue of capillary condensation occurs such that the cavities are rapidly filled by the liquid. In the case of the parabolically shaped cavities, however, $\Delta\mu_{\rm fil}^{p,g}$ marks the crossover from the power-law filling regime at $\Delta\mu > \Delta\mu_{\rm fil}^{p,g}$, to the postfilling one. If we denote the equilibrium interface height at the position of the symmetry axes of the cylindrical or parabolic pits as $l_p^{(0)}$, and in the middle of the rectangular or parabolic grooves as $l_g^{(0)}$, we obtain in the postfilling regime

$$l_{p,g}^{(0)}(\Delta\mu, R, P, D) = R\Lambda_{p,g}((\Delta\mu/\varepsilon_f)(R/\sigma)^{1+\delta}), \quad (1)$$

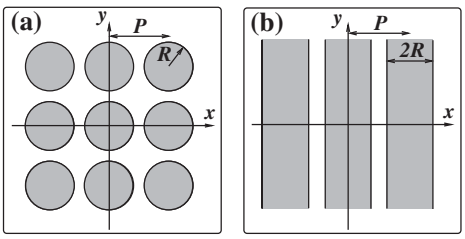

FIG. 1. Top view of the substrate geometries. (a) Quadratic lattice of identical pits (cylinders or paraboloids). (b) Periodic array of grooves (rectangular or parabolic). All cavities have finite depths D.

$$\Lambda_p(x) = \Lambda_g(x/2). \quad (2)$$

Here ε_f and σ are a molecular energy and length scales, respectively. Equation (2) expresses the same covariance relation as the one reported in Ref. [9]. The scaling functions $\Lambda_{p,g}(x)$ do not depend on D and P; i.e., in this regime $l^{(0)}_{p,g}$ increases upon decreasing undersaturation in the same way for an isolated cavity as for arrays of them.

We base our calculations on the effective interface Hamiltonian description [10]

$$H[l] = \iint d^2x(\sigma_{lg}\sqrt{1+(\nabla l)^2} + \Delta\mu\Delta\rho l + W(\mathbf{x}, l)), \quad (3)$$

where $l(\mathbf{x})$ denotes the local interfacial height which is measured from the plane $z = 0$ where the substrate ends, $\mathbf{x} \equiv (x, y)$ denotes the lateral coordinates, σ_{lg} is the surface tension of the free liquid-vapor interface, $\Delta\rho = \rho_l - \rho_g$ is the difference in number densities of the coexisting bulk phases, and $W(\mathbf{x}, l)$ is the effective interface potential. The functional in Eq. (3) can be derived systematically from microscopic density functional theory, which allows one to determine the explicit functional form of $W(\mathbf{x}, l)$ for a given substrate shape and its dependence on the fluid-fluid and substrate-fluid interaction potentials. We approximate the attractive parts of the pair potentials by $\phi_{f,s}(r) = -\frac{128\sqrt{2}}{9\pi}\varepsilon_{f,s}\sigma^6(\sigma^2 + r^2)^{-3}$. The amplitude is chosen such that the integrated strength of ϕ_f equals that of the attractive contribution of the Lennard-Jones potential obtained by a strict application of the Weeks-Chandler-Andersen procedure. This leads to the effective interface potential

$$W_\Omega(\mathbf{x}, l) = A \times I_\Omega(\mathbf{x}, l),$$
$$I_\Omega(\mathbf{x}, l) = \int_l^\infty dz \int_\Omega d^3r'(\sigma^2 + |\mathbf{r} - \mathbf{r}'|^2)^{-3}, \quad (4)$$

where $A = -\frac{128\sqrt{2}}{9\pi}\sigma^6\Delta\rho(\rho_l\varepsilon_f - \rho_s\varepsilon_s) > 0$ is an effective Hamaker constant with ρ_s as the number density of the substrate, and Ω denotes the domain occupied by substrate particles. The effective interface potential of the planar substrate is $W_\pi(l \gg \sigma) \approx A\pi/(12l^2)$, so that $l_\pi(\Delta\mu \to 0) = (A\pi/(12\Delta\rho\Delta\mu))^{1/3}$.

In the following, we minimize the functional in Eq. (3) numerically, which yields the equilibrium interface height $l(\mathbf{x})$ within mean-field theory which is valid in $d = 3$ for complete wetting [10] and filling [9] for the dispersion forces considered here. For all substrate geometries the midpoint heights $l^{(0)}_{p,g}(\Delta\mu)$ exhibit four different regimes.

The first regime corresponds to the *filling* of the cavities. For the case of rectangular grooves and cylindrical pits, and for D/R large enough, a quasiabrupt, but still continuous filling of the cavities takes place at $\Delta\mu = \Delta\mu^{p,g}_{\text{fil}}(R)$, which is shown in the inset of Fig. 2. A similar behavior has been reported earlier for an isolated rectangular groove [11]. We find numerically for $R/\sigma \gtrsim 50$ that $\Delta\mu^{p,g}_{\text{fil}}(R) \sim R^{-1-\delta}$, with an effective exponent $\delta \approx 0.035$ for both the rectangular grooves and the cylindrical

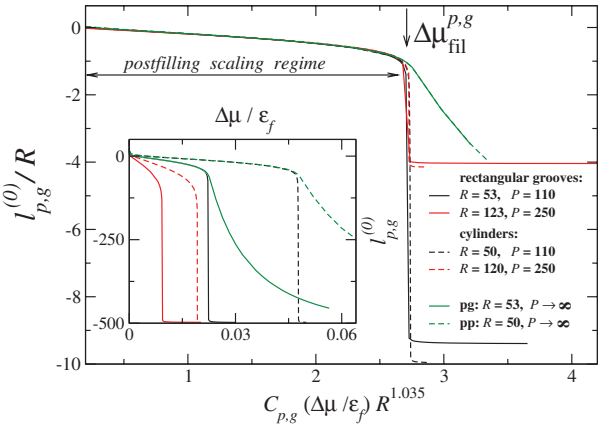

FIG. 2 (color). Typical interfacial heights $l^{(0)}_{p,g}$ (measured from the plane $z = 0$) at the middle of the cylindrical and parabolic pits, $l^{(0)}_p$ (dashed lines), and of the rectangular and parabolic grooves, $l^{(0)}_g$ (solid lines), as a function of $\Delta\mu$ with $C_p = 1$ and $C_g = 2$. Rescaling the variables according to Eq. (1) leads to data collapse. The inset shows the same data unscaled. The depth of the cavities is $D = 500$; $pp(g)$ denotes parabolic pits (grooves). All lengths are measured in units of σ.

pits. The locus of the filling transformation satisfies also the relation $\Delta\mu^p_{\text{fil}} = 2\Delta\mu^g_{\text{fil}}$. In the case of parabolic cavities, complete filling is described by an effective power law, $l^{(0)}_{p,g}(\Delta\mu, R, D) \sim \Delta\mu^{-\gamma(R,D)}$ valid for $\Delta\mu \gtrsim \Delta\mu^{p,g}_{\text{fil}}$. We find the values of the effective exponent γ ranging from ca. 3.1, for $R = 245\sigma$, to ca. 2.0, for $R = 50\sigma$, at a cavity depth $D = 500\sigma$. Moreover, the complete filling of the parabolic cavities obeys the covariance relation $l^{(0)}_p(\Delta\mu, R, D) = l^{(0)}_g(\Delta\mu/2, R, D)$.

In the second, *postfilling regime*, i.e., for $\Delta\mu \in (\Delta\mu^e_\pi, \Delta\mu^{p,g}_{\text{fil}})$, the midpoint height for all patterns shows an almost linear dependence on $\Delta\mu$ on normal scales. The morphologies of the liquid films still reflect the geometrical patterns; i.e., there are considerable lateral variations of the interfacial heights. We find that the slopes of the $l^{(0)}_{p,g}$ curves scale as R^α with $\alpha \approx 2$. Thus, combining this fact with the scaling of the filling chemical potential $\Delta\mu^{p,g}_{\text{fil}}$, we propose for the functions $l^{(0)}_{p,g}$ in the postfilling regime the scaling forms given by Eq. (1). The scaling functions $\Lambda_{p,g}$ and the corresponding data collapse upon suitably rescaling the chemical potential are shown in Fig. 2. The scaling functions $\Lambda_{p,g}$ in the postfilling regime do not depend on the cavity depth D and the pattern periodicity P. In the case of a single cavity, i.e., in the limit $P \to \infty$, we obtain the same curves $l^{(0)}_{p,g}(\Delta\mu)$ as those presented in Fig. 2.

Below a certain value $\Delta\mu^e_\pi$ the interface height becomes de facto flat, denoted as $l_{p,g}$ for the respective patterns. In the case of the rectangular grooves or cylindrical pits, $\Delta\mu^e_\pi$ marks the crossover from the postfilling scaling regime to the *effective planar scaling regime* within which the wetting behavior of geometrically patterned substrates can be mapped onto that of layered flat solids. The upper layer of

those solids has a thickness D, and its composition is related to the geometrical parameters R and P. For the flat interfaces the functional in Eq. (3) reduces to a function of $l_{p,g}$, the minimum of which determines the thicknesses of the wetting films in this regime. Figure 3 shows the functions $l_g(\Delta\mu)$ for several values of R and P, as well as the liquid film thickness $l_\pi(\Delta\mu)$ adsorbed on the corresponding planar substrate. The rectangular groove (and cylindrical pit, not shown) geometries lead to the same power-law behavior as for a flat surface, $l_{p,g} \sim \Delta\mu^{-1/3}$, but with different amplitudes reflecting different effective Hamaker constants, which depend on the geometry of the patterns. In order to find the geometrical dependence of the amplitudes of the scaling laws given above, we mimic sculptured substrates by layered and flat ersatz solids, with the effective interface potential $W(l \gg \sigma) \approx \frac{\pi}{12}(A^e/l^2 + (A - A^e)/(l + D)^2)$ [12]. The first term is the effective interface potential of a flat semi-infinite solid with Hamaker constant A^e and the second term is the correction due to the actual bottom part of the substrate, $z \in (-\infty, -D)$, with Hamaker constant A. For $\sigma \ll l \lesssim D$, to a good approximation, one may ignore the bottom part of the substrate [i.e., the second term in $W(l \gg \sigma)$] so that the amplitude is determined by the Hamaker constant A^e. Consider a lateral unit cell ω_0 of this sculptured part of the substrate ($z \in [-D, 0]$), with ω_s as its domain occupied by the solid. By requiring $W_{\cup\omega_s}(\mathbf{x}, l) = W^e_{\cup\omega_0}(\mathbf{x}, l)$, we obtain for the effective Hamaker constant $A^e = AI_{\cup\omega_s}(\mathbf{x}, l)/I_{\cup\omega_0}(\mathbf{x}, l)$, where $W^e_{\cup\omega_0}$ is the effective interface potential generated by the laterally homogeneous top layer

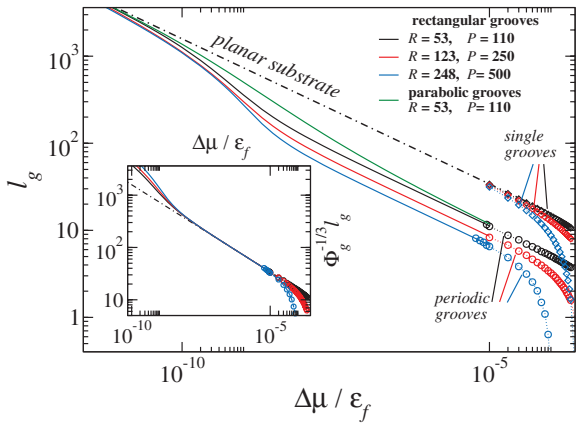

FIG. 3 (color). Wetting film thickness l_g above grooves for small $\Delta\mu$. The symbols represent the midpoint interfacial height $l_g^{(0)}$. The solid lines are obtained by minimizing Eq. (3) assuming $l(\mathbf{x}) = l_g$. On the present scales they are indistinguishable from those for film thicknesses $l^e_\pi(\Delta\mu)$ on layered and flat ersatz substrates, with a top layer of height D and an effective Hamaker constant $A^e = A\Phi_g$, where A is the Hamaker constant of the solid without grooves. In the inset the vertical axis is rescaled according to Eq. (6) leading to data collapse within an intermediate regime, the width of which increases as $\Delta\mu^e_\pi - \text{const} \times D^{-3}$ for $D \to \infty$. The groove depth is $D = 500$.

of the layered and flat ersatz substrate; the symbol $\cup$ denotes the union of domains. For $l \gg \sigma$ the integrals $I_{\cup\omega_i}$ ($i = s, 0$) can be approximated as

$$I_{\cup\omega_i} \approx \int_l^\infty dz \int_{\cup\omega_i} \frac{d^3r'}{(z - z')^6}\left(1 - 3\,\frac{\sigma^2 + \|\mathbf{x} - \mathbf{x}'\|^2}{(z - z')^2}\right). \tag{5}$$

In Eq. (5) the leading term as a function of l renders $A^e \approx AS_s/S_0$, where S_i is the surface area of the domain $\omega_i \cap \{(\mathbf{x}, z = 0)\}$. Thus, we obtain $A^e_g \approx A\Phi_g$ for the rectangular grooves and $A^e_p \approx A\Phi_p$ for cylindrical pits. $\Phi_g = 1 - 2R/P$ and $\Phi_p = 1 - \pi(R/P)^2$ are the areal fractions of solid in the top layer, $z = 0$, of substrates with rectangular groove and cylindrical pit patterns, respectively. The thicknesses $l^e_\pi(\Delta\mu)$ of the wetting films on such layered ersatz substrates, which effectively correspond to arrays of grooves, are almost indistinguishable from the corresponding ones for l_g. In the case of a lattice of cylindrical pits we observe the same behavior of the corresponding l_p curves (not shown). Therefore, we conclude that, for sufficiently thick wetting films, $l_{p,g}$ obeys the following scaling relation:

$$l_{p,g}(\Delta\mu, R, P, D) = (\Phi_{p,g})^{1/3} l_\pi(\Delta\mu), \tag{6}$$

where l_π is the thickness of the wetting film on the planar substrate. Indeed, after rescaling by the geometry-dependent factors $(\Phi_g)^{-1/3}$, the curves for l_g collapse and, within the numerical precision, coincide with the curve for l_π. This is shown in the inset of Fig. 3. Equation (6) is reminiscent of the Cassie equation [13] describing the apparent contact angle on chemically structured substrates.

As l_g reaches the value $\sim D$, i.e., at $\Delta\mu = \Delta\mu_\pi \sim D^{-3}$, a crossover to the *planar scaling regime* takes place. In the planar scaling regime, $\Delta\mu \lesssim \Delta\mu_\pi$, the geometrical patterns are irrelevant. This crossover occurs only for long-ranged dispersion forces. (For short-ranged interactions, instead, the growth of the wetting film would remain determined by the areal fraction of solid at $z = 0$ for all film thicknesses.) For $D \to 0$, $\Delta\mu_\pi$ merges with $\Delta\mu^e_\pi$, and the width of the effective planar regime, i.e., the range of applicability of Eq. (6) vanishes. In the case of the parabolic pits and grooves, we do not observe the effective planar scaling regime. There is rather an extended crossover region from the postfilling scaling regime to the planar one, see Fig. 3.

Figure 4 compares our results with the corresponding experimental data of Ref. [4], in which the adsorption of methylcyclohexane (MCH) on a silicon substrate sculptured by a hexagonal lattice of parabolic pits has been studied with the following geometrical parameters: depth $D \approx 200$ Å; radius of the pits at the opening $R \approx 123$ Å; lattice constant $P \approx 394$ Å. As in Ref. [4], we display the volume $\Gamma = \Gamma_p + \Gamma_t$ of adsorbed liquid divided by the projected area and multiplied by the electron density of

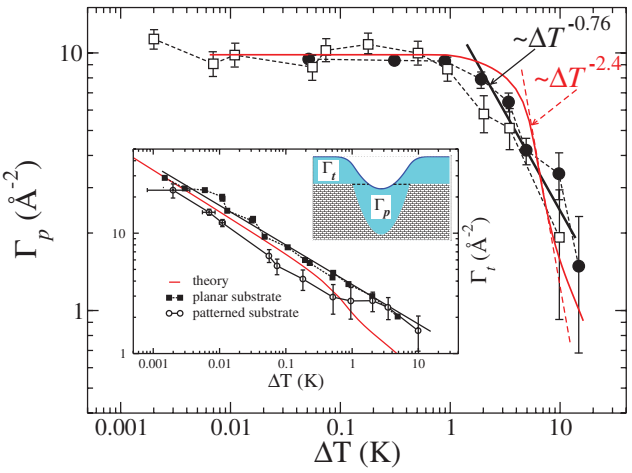

FIG. 4 (color). Liquid adsorption at parabolic pits. Inset: $\Gamma_t(\Delta T)$. Red line—theory; symbols and black lines—experimental data from Ref. [4] (where Γ_p is denoted as Γ_c). ΔT is proportional to $\Delta\mu$ (see main text).

the bulk fluid as the sum of the amount Γ_p adsorbed in the pit, and the amount Γ_t adsorbed above the pit opening. For MCH we adopt the Lennard-Jones parameters $\sigma = 5.511$ Å and $\varepsilon_f/k_B = 446$ K [14]. Then the relation between the undersaturation $\Delta\mu$ and the reservoir-substrate temperature difference (used in the experiment as a means to tune the deviation from liquid-vapor coexistence) is $\Delta T \approx 32.37 \frac{\Delta\mu}{\varepsilon_f} K$. Fitting the film thickness on the planar substrate to the corresponding experimental curve fixes the value of the Hamaker constant. For the liquid-vapor surface tension of MCH we use $\sigma_{lg} = 22.72 \frac{\text{dyn}}{\text{cm}}$ for $T = 30\,^\circ\text{C}$ [15]. Adjusting the geometry of the patterns to the experimental ones we calculate Γ_p and Γ_t as functions of ΔT. We emphasize that at this stage there are no free parameters left in the model.

The resulting curves are shown in Fig. 4. For both quantities we obtain good quantitative agreement with the experimental results. In the filling regime ($5\text{ K} \lesssim \Delta T \lesssim 8\text{ K}$) the calculated $\Gamma_p(\Delta T)$ exhibits a power-law behavior $\Gamma_p \propto \Delta T^{-\beta_p}$ with an effective exponent $\beta_p \approx 2.4$. The apparent disagreement with the value $\beta_p \approx 0.76$ used in Ref. [4] can be explained by the mislocation of the filling regime on the experimental $\Gamma_p(\Delta T)$ curve due to the large error bars for the data points at large ΔT. The weak crossover at $\Delta T \approx 8$ K corresponds to the disappearance of the interfacial meniscus, so that for larger values of ΔT the interface follows the shape of the substrate. We have found that for larger cavities this crossover becomes more pronounced and for sufficiently large D and R we obtain the exponent $\beta_p = 3.4$. Thus, our results suggest that, in order to observe experimentally a more pronounced effective power law describing the filling of the cavities, much deeper and larger pits should be studied. There seems to be a difference between the behavior of the theoretical and experimental Γ_t for large ΔT. However, for such large undersaturations the wetting film is only ca. 10 Å thick, causing rather large error bars (actually larger [16] than those presented in the inset of Fig. 4) for extracting values for the adsorption from the scattering data.

In summary, as a function of undersaturation, we have studied complete wetting of four classes of substrates structured by one- and two-dimensional periodic patterns of fixed depth and we have identified four scaling regimes. The filling and the postfilling evolutions of the interfacial profiles do not depend on the periodicity of the patterns, but are determined by a single isolated cavity. For sufficiently deep structures there exists a range of undersaturations, in which the midpoint interfacial heights, obtained for different patterns, can be expressed in terms of a single scaling function. For small undersaturations, the single-cavity behavior crosses over to one dominated by the presence of many of them, for which the interfacial thickness increases as on a planar substrate, but characterized by an effective geometry-dependent Hamaker constant. Ultimately, for very small undersaturations the wetting film thickness becomes independent of the geometrical substrate structures.

It is our pleasure to acknowledge correspondence with Ben Ocko and Peter Pershan.

[1] T. Yanagishita, K. Nishio, and H. Masuda, Adv. Mater. **17**, 2241 (2005).
[2] E. Martines, K. Seunarine, H. Morgan, N. Gadegaard, C. D. W. Wilkinson, and M. O. Riehle, Nano Lett. **5**, 2097 (2005).
[3] E. Delamarche, D. Junker, and H. Schmid, Adv. Mater. **17**, 2911 (2005), and references therein.
[4] O. Gang, K. J. Alvine, M. Fukuto, P. S. Pershan, C. T. Black, and B. M. Ocko, Phys. Rev. Lett. **95**, 217801 (2005).
[5] L. Bruschi, A. Carlin, and G. Mistura, Phys. Rev. Lett. **89**, 166101 (2002).
[6] C. Rascón and A. O. Parry, Nature (London) **407**, 986 (2000); J. Chem. Phys. **112**, 5157 (2000).
[7] A. O. Parry, M. J. Greenaal, and J. M. Romero-Enrique, Phys. Rev. Lett. **90**, 046101 (2003).
[8] D. B. Abraham, A. O. Parry, and A. J. Wood, Europhys. Lett. **60**, 106 (2002).
[9] C. Rascón and A. O. Parry, Phys. Rev. Lett. **94**, 096103 (2005).
[10] S. Dietrich, in *Phase Transitions and Critical Phenomena*, edited by C. Domb and J. L. Lebowitz (Academic, New York, 1988), Vol. 12, p. 1.
[11] G. A. Darbellay and J. M. Yeomans, J. Phys. A **25**, 4275 (1992).
[12] M. O. Robbins, D. Andelman, and J. F. Joanny, Phys. Rev. A **43**, 4344 (1991).
[13] A. B. D. Cassie, Discuss. Faraday Soc. **3**, 11 (1948).
[14] S. Goldman, J. Phys. Chem. **80**, 1697 (1976).
[15] J. J. Jasper, J. Phys. Chem. Ref. Data **1**, 841 (1972).
[16] O. Gang, P. S. Pershan, and B. M. Ocko (private communication).